RESEARCH ARTICLE

Check for updates

Janus hollow polymeric hairy microspheres as efficient adsorbents and catalyst scaffolds†

Guang Wu,[a] Lingling Zhao, (ID) *[ab] Hongze Liang,[a] Yinghua Yan (ID) [a] and Hui Tan*[b]

Polymeric hairy microspheres with a Janus hollow structure were prepared *via* cationic polymerization using SiO_2 nanoparticles as interface protection cores and sacrificial templates. Sulfonic acid groups ($-SO_3H$) were introduced onto the surface of the microspheres by sulfonation and facilitated the further loading of titania. The Janus hollow polymeric hairy microspheres (HSPHS) could be applied as efficient adsorbents to remove both hydrophilic dye rhodamine B (RB) and hydrophobic dye dimethyl yellow (DMY) from the surrounding solution, and the results showed that >98% of RB or/and DMY could be removed within several minutes. The maximum adsorption amount on the Janus HSPHS was 3.48 and 0.14 mol g^{-1} for RB and DMY, respectively. In addition, the HSPHS can also serve as catalyst scaffolds to load anatase titania for the photocatalytic degradation of RB. Janus hollow microspheres coated with anatase titania (HSPHS@TiO_2-An) demonstrated a remarkable photocatalytic efficiency and recyclability. High photocatalytic activity was observed for HSPHS@TiO_2-An and the catalytic efficiency remained with almost no loss of the photocatalytic activity even after five catalytic cycles. Thus, the Janus hollow polymeric hairy microspheres have promising applications in water treatment as efficient adsorbents and catalyst scaffolds.

Introduction

Nowadays, with the increased development of industrialization and technology, water pollution caused by a large amount of wastewater discharged from factories has a serious influence on the environment and human health.[1,2] As organic dyes widely used in the paper, textile, coating, dying, printing and related industries are one of the most common contaminations in wastewater responsible for pollution problems, the removal of dyes from wastewater is required for environmental protection.[3,4] Therefore, various treatment technologies including biological (aerobic processes, anaerobic processes and combined aerobic–anaerobic processes),[5–7] chemical (electrochemical or advanced oxidation, photo-catalysis or sonolysis)[8,9] and physical (membrane separation and adsorption)[10,11] methods have been explored to remove dyes from wastewater. Among these methods, adsorption and catalysis techniques have attracted much attention due to their high efficiency, convenient operation and cost-effectiveness.[12,13]

A number of adsorbents have been applied to remove dyes from wastewater. For example, low-cost adsorbents produced on the basis of agricultural wastes, natural compounds and activated carbon have been used to remove pollutants indiscriminately,[14–17] while their adsorption capacities, mechanical strength and other properties need further improvement.[18] Many conventional porous materials such as activated carbon,[19–21] zeolites[22,23] and nanotubes[24,25] have been extensively used to adsorb pollutants for water cleaning, while they have the disadvantages of low adsorption capacity and removal efficiency.[26] Due to the high surface area, good mechanical strength, adjustable surface chemistry and easy regeneration, polymeric adsorbents are potential candidates to remove different pollutants from aqueous media, and the adsorption capacity of polymeric adsorbents could be improved by using functional monomers to bound target pollutants with the polymeric matrix *via* specific interactions.[18,27] In recent years, covalently linked porous polymers such as conjugated nano-/mircoporous polymers,[28,29] covalent organic frameworks,[30] hyper cross-linked polymers[31,32] and synthetic functional copolymers[33,34] have aroused much attention and been successfully applied in adsorption due to their vast surface area, low density and feasible functionality.

In addition, porous polymeric microspheres with high specific surface areas and physicochemical stability are attractive adsorbents in the application of water treatment.

[a] *School of Materials Science and Chemical Engineering, Ningbo University, Ningbo, 315211, China. E-mail: zhaolingling@nbu.edu.cn*

[b] *Health Science Center, The First Affiliated Hospital of Shenzhen University, Shenzhen, 518035, China. E-mail: huitan@email.szu.edu.cn*

† Electronic supplementary information (ESI) available: Synthetic conditions of SiO_2@PHS, SiO_2@SPHS and HSPHS; FT-IR spectra; EDX spectra; adsorption kinetics of RB with HSPHS; adsorption percentage of RB with HSPHS; adsorption kinetics of DMY with HSPHS; adsorption percentage of DMY with HSPHS; photocatalytic degradative capacity of RB. See DOI: 10.1039/c9qm00057g

Yao and coworkers[35] reported porous magnetic polyacrylamide microspheres for efficient removal of methylene blue with high adsorption efficiency and capacity. The adsorbed dyes can be easily desorbed from the magnetic polyacrylamide microspheres, and the polymeric microsphere adsorbents can be repeatedly used for at least 6 cycles without losing the adsorption capacity. Chen et al.[36] designed and fabricated novel dual-functionalized hollow polymer particles (DF-HPP) as a high-performance adsorbent for selective removal of methylene blue. The DF-HPPs exhibited excellent adsorption properties with high adsorption capacity, fast adsorption/desorption rates, unique pH-sensitivity and easy recovery due to the high density of carboxylate and amino groups as well as the high surface area.

Apart from being good adsorbent candidates, porous polymeric microspheres can also serve as catalyst scaffolds and have gained extensive attention in the past few decades.[12,37] Wang et al.[38] fabricated novel chitin microspheres as the enabling platform for a range of applications including as a recyclable catalyst support and adsorbent. The swollen porous polymer could successfully control the growth of gold nanoparticles and reduced the dimensions of metal particles ($r \leq 5$ nm). The chitin/Au nanocomposite microspheres served as adsorbents for enhanced removal of methylene blue from aqueous solution. Yang et al.[39] prepared porous poly(styrene-divinylbenzene) microspheres with an interconnected structure for effective adsorption of dyes in an aqueous solution, and the Ag-loaded hybrid microspheres exhibited excellent catalytic degradation of the dyes. Very recently, hierarchical porous spheres with a special structure have attracted another wave of interest in the fabrication of functional materials because of their functional properties.[40,41] Ning et al.[12] developed a novel kind of polymeric microsphere with a hierarchical porous structure (HPPMs) based on double Pickering emulsion templates. The HPPMs can be employed as an effective adsorbent for rhodamine 6G. The hierarchical porous structure of the HPPMs can offer loading sites for Ag particles as well as protect the Ag particles from aggregation. Thus, the noble metal loaded HPPMs maintained an outstanding performance in catalysis and recyclability.

Herein, we developed a novel kind of polymeric hairy microsphere with a Janus hollow structure *via* cationic polymerization using SiO2 nanoparticles as the interface protection cores and sacrificial templates, in which the interior cavity was hydrophobic and the exterior surface was hydrophilic and connected with polymeric tubular fibers. Sulfonic acid groups were introduced into the exterior surface of the microspheres by sulfonation and facilitated the further loading of titania; thus, the Janus hollow polymeric hairy microspheres can serve as efficient adsorbents as well as catalyst scaffolds. So far, most of the reported adsorbents for water cleaning can remove the basic or cationic dyes from wastewater,[19,42] such as methyl blue basic yellow 21, basic red 22, Congo red, rhodamine B and rhodamine 6G, and these synthetic organic dyes are water soluble dyes. However, the contaminating dyes discharged from factories into water include not only water-soluble (hydrophilic) dyes but also water-insoluble (hydrophobic) dyes.[15]

Therefore, the removal of both hydrophilic and hydrophobic dyes from wastewater is of great importance for water cleaning and environment protection. The novel Janus hollow polymeric hairy microspheres with a hydrophobic interior cavity and a hydrophilic surface can remove both hydrophilic and hydrophobic dyes from wastewater, and the further loaded titania can serve as a photocatalyst to degrade the contaminated dyes in the wastewater. In this work, the fabrication and characterization of Janus hollow polymeric hairy microspheres were demonstrated and the adsorption and catalytic properties were evaluated.

Experimental

Materials

Divinylbenzene (80%) (DVB) and hydrofluoric acid (40%) (HF) were purchased from Aladdin Reagent Company. Boron trifluoride diethyl etherate complex (BF3·O(Et)2) was purchased from TCL (Shanghai) Development Co, Ltd. Tetraethyl orthosilicate (TEOS), dimethyl yellow (DMY), alkaline alumina, concentrated sulfuric acid (H2SO4, 95–98%), ammonium hydroxide (NH3·H2O, 28%), span 80, anhydrous ethanol and *n*-hexane were purchased from Sinopharm Group Chemical Reagent Co., Ltd, China. Tetrabutyl titanate (TBOT) was purchased from Shanghai Macklin Biochemical Co., Ltd, China. Rhodamine B (RB) was purchased from Shanghai Yuanye Biochemical Co., Ltd, China.

Preparation of the SiO2 cores

SiO2 nanospheres with the diameter of 400 nm were synthesized by the alkaline hydrolysis of TEOS *via* the well-know Stöber method. Briefly, 40 mL of anhydrous ethanol, 2.7 mL of deionized water and 4 mL of ammonium hydroxide were added to a flask in sequence under room temperature. The mixture was stirred for 20 min to form a uniform solution and then 3.3 mL of TEOS was added and stirred for another 6 h at room temperature. The precipitate was centrifuged and washed with deionized water until the pH was neutral. The SiO2 nanospheres were dried at 60 °C and stored at room temperature for further use.

Preparation of SiO2@polymeric hairy spheres (SiO2@PHS)

SiO2@PHS was produced by polymerization of the DVB on the surface of the SiO2 cores. The DVB was filtered with alkaline alumina to remove the inhibitor before use. Typically, 10 mg of SiO2 nanospheres were dispersed ultrasonically in 50 mL of *n*-hexane in a 100 mL flask. 59 mg of span 80 was added to the dispersion and mixed uniformly. Then, 54 μL of BF3·Et2O was added and the mixture gradually turned yellow. Next, 550 μL of DVB was added to react for several minutes and then anhydrous ethanol was added to quench the reaction. A white precipitate was generated at the bottom of the flask. The product was washed with ethanol three times and dried at room temperature. SiO2@PHS with different morphologies could be obtained by changing the feed ratio of span 80, BF3·Et2O and DVB as well as the reaction time.

This journal is © The Royal Society of Chemistry and the Chinese Chemical Society 2019

Mater. Chem. Front., 2019, **3**, 922–930 | 923

Preparation of SiO₂@sulfonated polymeric hairy spheres (SiO₂@SPHS)

SiO₂@SPHS was achieved by the following process. 400 mg of SiO₂@PHS was dispersed into 10 mL of concentrated sulfuric acid at room temperature for several hours; next, the microspheres were washed with a large amount of ethanol and deionized water to remove the sulfuric acid and then dried at 60 °C. The harvested light yellow product was stored at room temperature for further use.

Preparation of Janus hollow sulfonated polymeric hairy spheres (HSPHS)

HSPHS was produced by etching the SiO₂ cores of SiO₂@SPHS with HF. Typically, 150 mg of SiO₂@SPHS with different sulfonated times was dispersed in 4 mL of HF (2%) and ultrasonicated for 4 min. Then, the reaction was terminated with ammonia and the polymeric spheres were washed several times with deionized water and then dried at 60 °C. The harvested light yellow product was stored at room temperature for further use.

Preparation of titania encapsulated HSPHS (HSPHS@TiO₂)

Encapsulation of the HSPHS with titania was performed according to previously reported work.[43] 1.5 mL of TBOT was dispersed in 10 mL of anhydrous ethanol, and then the mixture was added dropwise into 10 mL of ethanol suspension containing 50 mg of HSPHS-3 under stirring. 2 mL of distilled water was dropped into the mixture and stirred for another 6 h. The microspheres were washed several times with ethanol and deionized water and then dried at room temperature. The sample was coded as HSPHS@TiO₂-Am. The crystallization treatment of the as-prepared amorphous titania was performed by the hydrothermal method.[44] 50 mg of HSPHS@TiO₂-Am was added to a Teflon-lined autoclave with 20 mL of deionized water, and the autoclave was sealed and placed in an oven at 180 °C for 2 h. After cooling down to room temperature, the microspheres were centrifuged and washed with deionized water, and then dried at room temperature. The sample was coded as HSPHS@TiO₂-An.

Characterization

Scanning electron microscopy (SEM, FEI Nova NanoSEM 450, 5 kV) and transmission electron microscopy (TEM, JEOL JEM2100, 200 kV) were conducted to observe the morphology of the samples. The surface composition of the microspheres was tested using energy-dispersive X-ray spectroscopy (EDX) on SEM. Infrared absorption spectra of the samples were measured using a Nicolet 6700 spectrometer with the sample/KBr pressed pellets. The XRD pattern was collected using a Bruker D8 Focus X-ray diffractometer. Thermogravimetric analysis was performed on a TG/DTA (Diamond, PerkinElmer) with a heating rate of 10 °C min⁻¹ from room temperature to 800 °C under an air atmosphere.

The Janus character of the HSPHS was characterized using a confocal laser scanning microscope (CLSM, Olympus FV1000). The HSPHS was dispersed in the aqueous solution of RB (50 mg L⁻¹) for 10 min to achieve saturation adsorption. The HSPHS was

collected *via* centrifugation and re-dispersed in water. A drop of HSPHS aqueous dispersion was dropped onto a microscope slide and covered with a coverslip. The slides were observed under CLSM with an excitation wavelength of 488 nm and an emission wavelength range of 510–600 nm.

Adsorption abilities of HSPHS

Adsorption of hydrophilic dyes using HSPHS. RB, a hydrophilic dye, was selected as a model compound for the adsorption test. 5 mg of the HSPHS was dispersed in 20 mL of RB aqueous solution (50 mg L⁻¹) and then the mixture was divided into five equal parts and incubated at room temperature to allow dye adsorption. At a predicted time, the supernatant was centrifuged, collected and measured using UV-visible spectroscopy (TU-1901).

The adsorption isotherms were obtained by batch equilibrium experiments. In detail, a series of 1 mg of HSPHS was dispersed in 4 mL of RB solution with concentrations ranging from 10 to 800 mg L⁻¹, respectively. The dispersion was centrifuged after incubating at room temperature for 10 min. The supernatant was collected and measured using UV-visible spectroscopy (TU-1901) to determine the residual dye concentration. The amounts of the adsorbed RB were calculated using the following equation: $Q_e = (C_0 - C_e) \times V/m$, where C_0 is the initial concentration of RB; C_e is the equilibrium concentration after adsorption; V is the solution volume and m is the mass of HSPHS. Photos were taken before and after adsorption.

Adsorption of hydrophobic dyes using HSPHS. DMY, a hydrophobic dye, was selected as a model compound for the adsorption test. 5 mg of the HSPHS was dispersed in 5 mL of deionized water, and then the dispersion was divided into five equal parts and each part was added into 1 mL of DMY hexane solution (20 mg L⁻¹). The mixture was ultrasonically shaken at room temperature and then held for equilibrated phase separation. At the predicted time, the hexane supernatant was centrifuged, collected and measured using UV-visible spectroscopy (TU-1901).

The adsorption isotherms were obtained by batch equilibrium experiments. A series of 1 mL of HSPHS aqueous dispersions (1 mg mL⁻¹) was added into 1 mL of DMY hexane solution with concentrations ranging from 5 to 50 mg L⁻¹, respectively. The mixture was ultrasonically shaken for 10 min and held for equilibrated phase separation. The hexane supernatant was centrifuged, collected and measured using UV-visible spectroscopy (TU-1901) to determine the residual dye concentration. The amounts of the adsorbed DMY were calculated using the following equation: $Q_e = (C_0 - C_e) \times V/m$, where C_0 is the initial concentration of the DMY hexane solution; C_e is the equilibrium concentration of the DMY hexane solution after phase transfer; V is the solution volume of hexane and m is the mass of HSPHS. Photos were taken before and after adsorption.

Adsorption of hydrophilic and hydrophobic dyes simultaneously using HSPHS. 4 mg of HSPHS was added into 4 mL of an ethanol solution containing 20 mg L⁻¹ DMY and 80 mg L⁻¹ RB. The mixture was incubated at room temperature. At the predicted time, the supernatant was centrifuged, collected and

measured using UV-visible spectroscopy (TU-1901). Photos were taken before and after adsorption.

Catalytic properties of HSPHS@TiO$_2$-An

Photocatalytic degradation kinetics. 7 mg of HSPHS-3, HSPHS@TiO$_2$-Am and HSPHS@TiO$_2$-An was dispersed in an aqueous solution of RB (50 mg L^{-1}) for 10 min to achieve saturation adsorption, respectively. The microspheres were centrifuged, collected and washed with water, and then re-dispersed in 0.7 mL of deionized water, respectively. Then, a series of 0.1 mL of microsphere aqueous dispersions (10 mg mL^{-1}) was added into 4 mL of RB aqueous solution (50 or 300 mg L^{-1}), respectively. The mixture was irradiated using a UV light (30 W, 254 nm) under stirring for photocatalytic degradation of the dye. At the predicted time, the supernatant was centrifuged, collected and measured using UV-visible spectroscopy (TU-1901). The kinetics of photocatalytic decolorization of the RB aqueous solution was expressed as $\ln(C_0/C) = kt$, where k is the apparent rate constant, C_0 is the initial concentration of RB and C is the concentration after UV irradiation.[44]

Photocatalytic degradation capacity. 8 mg of HSPHS-3, HSPHS@TiO$_2$-Am and HSPHS@TiO$_2$-An were dispersed in the aqueous solution of RB (50 mg L^{-1}) for 10 min to achieve saturation adsorption, respectively. The microspheres were centrifuged, collected and washed with water, and then re-dispersed in 0.8 mL deionized water, respectively. Then, a series of 0.1 mL of microsphere aqueous dispersions (10 mg mL^{-1}) was added into 4 mL of RB aqueous solution with concentrations ranging from 10 to 400 mg L^{-1}, respectively. The mixture was irradiated using a UV light (30 W, 254 nm) under stirring for 5 h. RB solution at the same concentration without any microspheres was used as a control. The supernatant was centrifuged, collected and measured using UV-visible spectroscopy (TU-1901). The amount of photodegradative RB was calculated using the following equation: De = $(C_0 - C_t) \times V$, where C_0 is the initial concentration of RB; C_t is the concentration after UV irradiation; V is the solution volume.

Regeneration of HSPHS@TiO$_2$-An. 1 mg of HSPHS@TiO$_2$-An was dispersed in an aqueous solution of RB (50 mg L^{-1}) for 10 min to achieve saturation adsorption. The microspheres were centrifuged, collected and washed with water, and then re-dispersed in 4 mL of RB aqueous solution (50 mg L^{-1}). The mixture was irradiated using a UV light (30 W, 254 nm) under stirring for 5 h. Then, the supernatant was centrifuged, collected and measured using UV-visible spectroscopy (TU-1901). The precipitate was re-dispersed in 4 mL of fresh RB aqueous solution (50 mg L^{-1}) and the same procedure was followed. The experiment was performed for five cycles.

Results and discussion

Preparation and characterization of SiO$_2$@PHS

SiO$_2$@PHS was prepared through a cationic polymerization initiated on the surface of SiO$_2$ cores. SiO$_2$@PHS with various morphologies can be obtained by changing the preparation
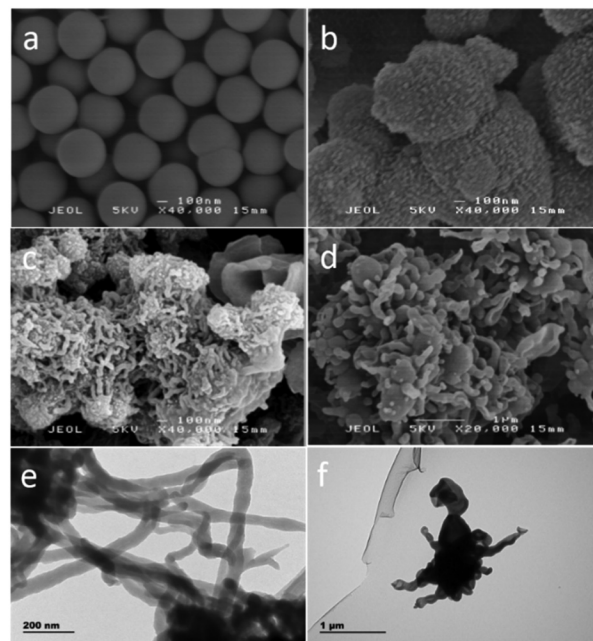

Fig. 1 SEM and TEM images of SiO$_2$ nanoparticles (a), SiO$_2$@PHS-1 (b), SiO$_2$@PHS-2 (c and e) and SiO$_2$@PHS-3 (d and f).

parameters (Table S1, ESI†). As shown in Fig. 1, the length of polymer fibers on the SiO$_2$@PHS surface increased as the polymerization time prolonged. After 1 min of polymerization, SiO$_2$@PHS with a very coarse surface containing short fibers was observed (SiO$_2$@PHS-1, Fig. 1b). When the polymerization time increased to 8 min, hairy SiO$_2$@PHS with longer fibers on the surface was obtained (SiO$_2$@PHS-2, Fig. 1c). The TEM image of the hairy part showed that the polymeric fiber has a bamboo-like structure and a diameter of $\sim$60 nm (Fig. 1e). When increasing the amount of initiator and keeping the other parameters constant, anthoid SiO$_2$@PHS with stumpy fibers on the surface was obtained (SiO$_2$@PHS-3, Fig. 1d). TEM showed that the fiber part has a hollow structure and a diameter of $\sim$150 nm (Fig. 1f).

Preparation and characterization of SiO$_2$@SPHS and HSPHS

SiO$_2$@PHS was sulfonated to introduce sulfonic acid groups (–SO$_3$H) on the surface of the microspheres and harvested a hydrophilic exterior layer in the polymeric hairy spheres. The interior surface of the polymeric hairy spheres was protected from sulfonation by the SiO$_2$ cores and resulted in a hydrophobic layer, thus the Janus shell was achieved. Subsequently, the SiO$_2$ cores were etched using HF to get Janus hollow
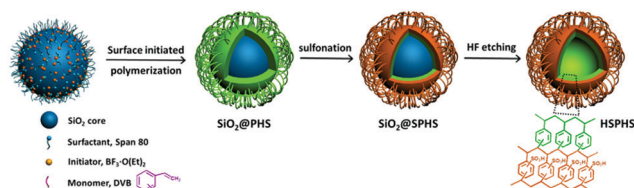
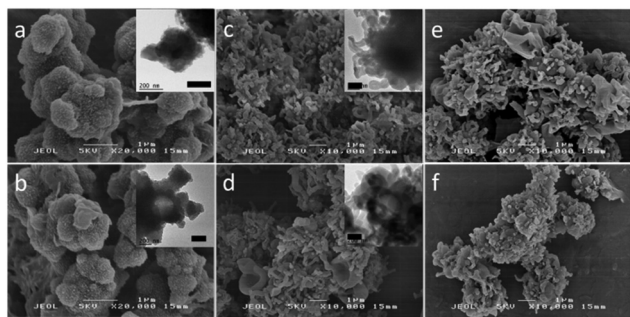**Scheme 1** Illustrative synthesis of the HSPHS.

Fig. 2 SEM images of SiO$_2$@SPHS and HSPHS. SiO$_2$@SPHS-1 (a), HSPHS-4 (b), SiO$_2$@SPHS-2 (c), HSPHS-2 (d), SiO$_2$@SPHS-3 (e) and HSPHS-3 (f). Insets are TEM images, bar = 200 nm.

Fig. 4 The SEM images of HSPHS@TiO$_2$-Am (a) and HSPHS@TiO$_2$-An (b), the XRD spectra of SiO$_2$@SPHS, HSPHS, HSPHS@TiO$_2$-Am and HSPHS@TiO$_2$-An (c), and the TGA analysis of HSPHS and HSPHS@TiO$_2$ (d).

polymeric hairy spheres, as shown in Scheme 1. In comparison with the SiO$_2$@PHS, new peaks at 1175 and 1025 cm^{-1} appear in the FTIR spectrum of SiO$_2$@SPHS (Fig. S1, ESI†), confirming that –SO$_3$H was successfully introduced to the polymeric hairy spheres.[45] The SEM images showed that the morphology of the polymeric hairy spheres has no significant change before and after sulfonation or HF etching, and the hollow structure was observed under TEM after the SiO$_2$ cores were removed by HF (Fig. 2). The Janus HSPHS indicated a ring-shaped fluorescent image under confocal laser scanning microscopy (CLSM) (Fig. 3a) when using water-soluble RB dye as a detector. This suggested that the RB molecules are selectively adsorbed onto the exterior surface because of the sulfonic acid groups. As a control, hollow polymeric hairy spheres prepared by first etching and then sulfonation were used to confirm the Janus shell. The CLSM displayed a sphere-shaped fluorescence image (Fig. 3b) when incubated with RB, indicating that the whole cavity of the hollow polymeric hairy spheres was hydrophilic without the protection of the SiO$_2$ cores.

Preparation and characterization of HSPHS@TiO$_2$

The introduction of –SO$_3$H on the polymeric spheres' surface facilitated the loading of titania. The SEM images of the

HSPHS@TiO$_2$ showed that the TiO$_2$ nanoparticles were coated onto the surface of the polymeric spheres and displayed coarse surfaces (Fig. 4). In comparison with the HSPHS, the HSPHS@TiO$_2$ displayed a new peak assigned to Ti in the EDX spectra (Fig. S2, ESI†), confirming the successful loading of titania. The XRD spectra showed that the as-prepared (or untreated) titania has an amorphous state and the titania could transfer to anatase type through hydrothermal treatment. As shown in Fig. 4c, the diffraction peaks at 2θ angles of 25.3, 37.9, 48.1, 54.5 and 62.7° could be assigned to those of the anatase TiO$_2$, reflecting (101), (004), (200), (105) and (204) crystalline planes (JCPDS No. 21-1272), respectively.[44,46] The TGA analysis demonstrated that the content of titania loaded in the HSPHS@TiO$_2$-Am and HSPHS@TiO$_2$-An was 77.5% and 70.0%, respectively (Fig. 4d).

Adsorption behavior of HSPHS

The exterior layer of the Janus HSPHS was sulfonated to endow them with sulfonic acid groups, which could adjust the amphipathicity and adsorb water-soluble molecules. Rhodamine B (RB), a cationic dye used in the chemical industry but harmful to human health, was selected as a model compound to evaluate the adsorption ability of the Janus HSPHS. The adsorption isotherms for RB on different Janus HSPHS were displayed by the Langmuir model, where the amount of equilibrium adsorption, Q_e, was plotted as a function of the equilibrium concentration in bulk solution, C_e. The results demonstrated that the morphology and sulfonation degree of the Janus HSPHS had an effect on the dye adsorption. As shown in Fig. 5a, the anthoid Janus HSPHS with stumpy fibers on the surface (HSPHS-2) showed a higher adsorption capacity than the hairy Janus HSPHS when the sulfonation time was the same (1 h), and the hairy Janus HSPHS with longer fibers on the surface (HSPHS-1) displayed a higher adsorption capacity than the Janus HSPHS with short fibers on the surface (HSPHS-4). The adsorption of RB on the Janus HSPHS can be described by the Langmuir equation: $Q_e = Q_{max}KC_e/(1 + KC_e)$,[47–49] where
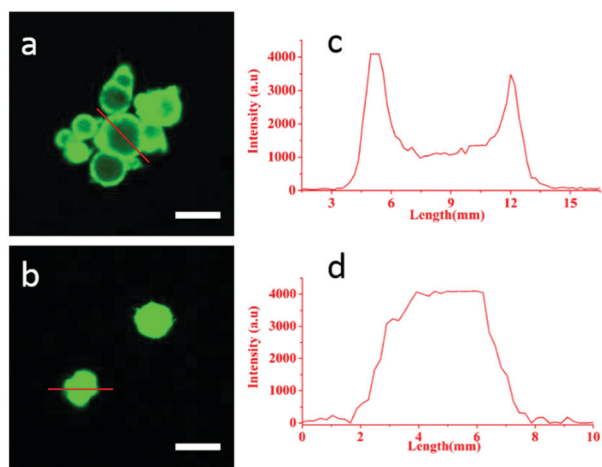

Fig. 3 CLSM images and the corresponding fluorescence intensity contours of the hollow polymeric hairy microspheres with (a and c) or without (b and d) Janus properties when incubated with RB. Bar = 2 μm.
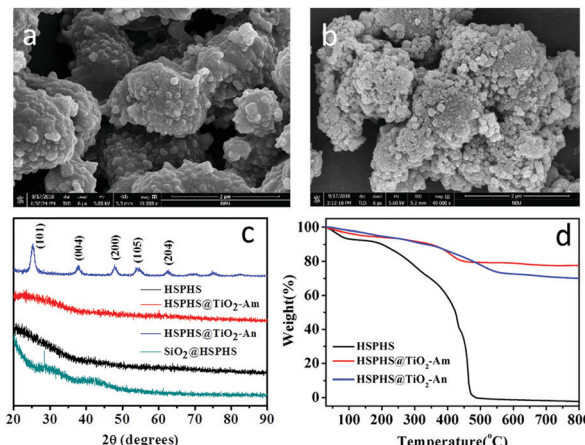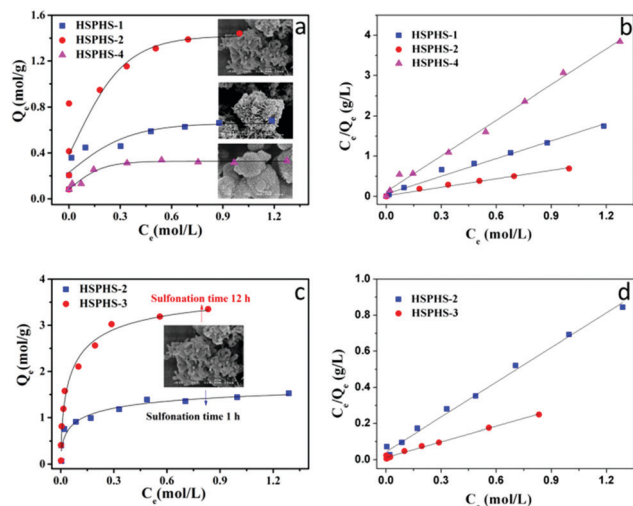
Fig. 5 The adsorption isotherms (a and c) of RB and the corresponding linear plots (b and d) using the Janus HSPHS with different morphologies (polymeric hairy) and sulfonation time at room temperature, respectively (HSPHS: 1 mg, RB aqueous solution: 4 mL).

Table 1 The Langmuir adsorption parameters of RB and DMY on the Janus HSPHS in solution

RB	Q_{max}^{a} (mol g^{-1})	K^{a} (M^{-1})	DMY	Q_{max}^{a} (mol g^{-1})	K^{a} (M^{-1})
HSPHS-1	0.68	23.29	HSPHS-2	0.14	16.10
HSPHS-2	1.43	36.28	HSPHS-3	0.11	13.64
HSPHS-3	3.48	22.91			
HSPHS-4	0.34	23.99			

^{a} The maximum adsorbed amount and the adsorption constant of RB or DMY on the Janus HSPHS were obtained by application of the Langmuir adsorption equation $Q_e = Q_{max}KC_e/(1 + KC_e)$.

Q_{max} is the maximum amount of adsorption, and K is the Langmuir adsorption constant. The adsorption parameters of Q_{max} and K can be easily obtained from Fig. 5b. It can be seen from Table 1 that the adsorption of RB on the Janus HSPHS provides a Q_{max} of 0.68, 1.43 and 0.34 mol g^{-1} for HSPHS-1, HSPHS-2 and HSPHS-4, respectively. In this, the anthoid Janus HSPHS with stumpy fibers on the surface was used in the following adsorption and photocatalytic degradation test. It is also found that the Janus HSPHS with a higher degree of sulfonation displayed a much higher adsorption capacity for RB (Fig. 5c), and the Q_{max} for RB using the anthoid Janus HSPHS with stumpy fibers on the surface increased from 1.43 to 3.48 mol g^{-1} when the sulfonation time increased from 1 h (HSPHS-2) to 12 h (HSPHS-3). This may be caused by the electrostatic interaction between the sulfuric acid group and the secondary amino group as well as the π–π interaction between the polymeric adsorbents and the dye molecule.[12,50] Besides, the adsorption kinetics test showed that the adsorption rate of RB on HSPHS-3 was very fast and as high as 99.8% of the RB was adsorbed within 2 min when the initial RB concentration was 50 mg L^{-1}, as shown in Fig. 6a.

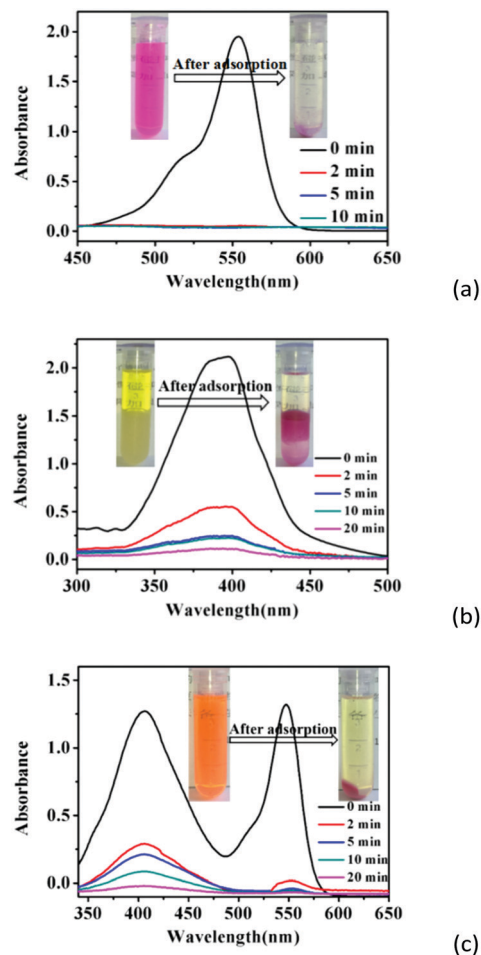The interior surface of the Janus HSPHS was hydrophobic PDVB without sulfonic acid groups due to the protection of the

Fig. 6 The UV-visible spectra of the RB aqueous solution (a) (HSPHS-3: 1 mg, RB aqueous solution: 50 mg L^{-1}, 4 mL), DMY solution in hexane (b) (HSPHS-3: 4 mg in 2 mL water, DMY solution in hexane: 20 mg L^{-1}, 2 mL), and RB and DMY solution in ethanol (c) (HSPHS-3: 4 mg, RB solution in ethanol: 80 mg L^{-1}, DMY solution in ethanol: 20 mg L^{-1}, 4 mL) adsorbed using the Janus HSPHS-3 as a function of time.

SiO$_2$ cores. Thus, the Janus HSPHS has different affinity on the interior and exterior surfaces, permitting a preferential capture of the hydrophobic species inside the cavity from their aqueous surrounding. Dimethyl yellow (DMY) was selected as a water-insoluble model compound to evaluate the capture ability of the Janus HSPHS. Upon mixing of the DMY solution in hexane and the Janus HSPHS aqueous suspension, the top hexane phase became less colorful and the bottom aqueous phase turned red due to the combination of captured DMY with sulfonic acid groups, as shown in Fig. 6b. The adsorption isotherms for DMY on the Janus HSPHS are presented in Fig. 7a, showing that the adsorption capacity was decreased with the sulfonation degree. The adsorption of DMY on the Janus HSPHS provides a Q_{max} of 0.14 and 0.11 mol g^{-1} for HSPHS-2 and HSPHS-3, respectively. The result was in contrary to the adsorption of water-soluble RB, possibly because the interior hydrophobic layer of Janus HSPHS decreased as the sulfonation degree increased, resulting in the reduced capture of water-insoluble DMY. The adsorption rate of DMY on HSPHS
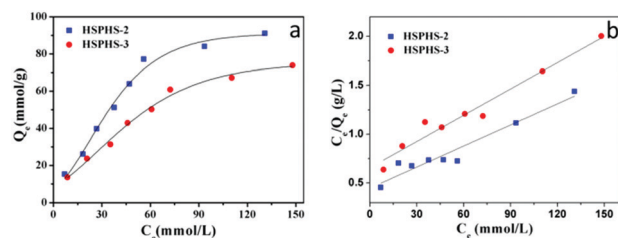
Fig. 7 The adsorption isotherms of DMY (a) and the corresponding linear plots (b) with different Janus HSPHS at room temperature (HSPHS: 1 mg in 1 mL of water, DMY hexane solution: 1 mL).
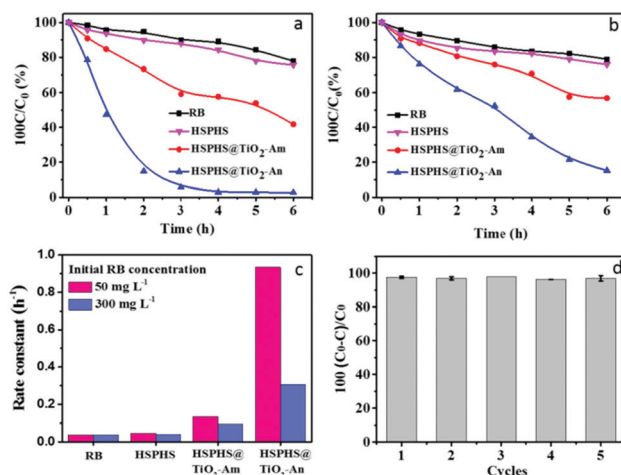

Fig. 8 Time course of the decrease in RB concentration under UV irradiation of 30 W. The initial RB concentration was 50 mg L^{-1} (a) and 300 mg L^{-1} (b) (catalyst 1 mg, RB solution 4 mL). Apparent rate constants (c). Cycling tests of the photocatalytic activity of HSPHS@TiO$_2$-An under UV light irradiation (d).

was very fast and the result demonstrated that as high as 98.2% of DMY molecules were captured within 20 min of ultrasonic mixing when the initial DMY concentration was 20 mg L^{-1}, as shown in Fig. 6b.

In addition, we also examined the adsorption ability of both water-soluble and water-insoluble molecules at the same time with the Janus HSPHS. The results showed that both RB and DMY dissolve in ethanol and could be adsorbed by HSPHS-3 simultaneously, displaying much less colorful solution after adsorption (Fig. 6c). The adsorption rate of both RB and DMY on the HSPHS was very fast and as high as 98.6% of RB and 97.1% of the DMY molecules were adsorbed within 20 min when the initial concentrations of RB and DMY were 80 and 20 mg L^{-1}, respectively, as shown in Fig. 6c.

Catalytic properties of the HSPHS@TiO$_2$

The Janus HSPHS with sulfonic acid groups make further metal oxide loading feasible, and titania was loaded to explore its application in catalyst systems. Water pollution with dyes is a significant problem to the environment and human health, and photocatalysis with TiO$_2$ containing scaffolds is an attractive approach to degrade the spent dyes. The photocatalytic activities of the samples were determined by photocatalytic degradation decolorization of RB in water under UV irradiation. The photolysis effect of RB without catalysts under UV irradiation was also checked. It was found that the amount of photodegradative RB increased with the initial concentration of RB when the amount of catalyst was kept constant, and the anatase titania encapsulated HSPHS (HSPHS@TiO$_2$-An) showed a much higher catalytic capacity compared with other samples (Fig. S8, ESI†). To evaluate the photocatalytic degradation rate of RB, the time course of the decrease in the concentration of RB was detected under light irradiation of 30 W, and the results are shown in Fig. 8. For the degradation of RB aqueous solution with low concentration (initial RB concentration was 50 mg L^{-1}), HSPHS without titania exhibited very low activity (rate constant, 0.0443 h^{-1}) as the RB (rate constant, 0.0377 h^{-1}) only, and the photodegradation ratio was 15.6% and 10.9% for the HSPHS and RB without catalyst respectively under 4 h of UV irradiation. The HSPHS coated with amorphous titania (HSPHS@TiO$_2$-Am) exhibited a decrease of 42.4% in the photodegradation ratio with a relatively low photocatalytic activity (rate constant, 0.1346 h^{-1}) due to the amorphous structure of coated titania.[51] For HSPHS coated with anatase titania (HSPHS@TiO$_2$-An), the highest photocatalytic

activity is observed with a rate constant of 0.9344 h^{-1}, and the photodegradation ratio of RB was 97.7% within 4 h (Fig. 8a and c). The highest photocatalytic activity of HSPHS@TiO$_2$-An is possibly due to the anatase crystallinity of the titania coated on the HSPHS. It's worth mentioning that when the initial concentration of the RB aqueous solution was increased to a fairly high level (300 mg L^{-1}), similar photodegradation of the RB solution was also observed while other parameters were kept constant. The HSPHS@TiO$_2$-Am exhibited a decrease of 42.4% in the photodegradation ratio with a rate constant of 0.0932 h^{-1}. The HSPHS@TiO$_2$-An exhibited a photodegradation ratio of 84.7% for RB, which exhibited a more rapid degradation process (rate constant, 0.3068 h^{-1}) than that of the HSPHS@TiO$_2$-Am, as shown in Fig. 8b and c.

As a catalyst, in addition to its catalytic efficiency, the recyclable catalytic ability is another important factor to be considered from the perspective of commercial application. Thus, the cycling photodegradation experiment of RB was performed to confirm the cyclic usage of HSPHS@TiO$_2$-An. The results demonstrated that the HSPHS@TiO$_2$-An possesses a remarkable catalytic efficiency and recyclability. As shown in Fig. 8d, a high catalytic efficiency of 97.7% is observed for the first cycle and the catalytic efficiency remains 97.0% with almost no loss of the photocatalytic activity after five catalytic cycles. It is well known that the photodegradation of TiO$_2$ is due to the photogenerated electrons and the holes. The negative conjugation effect shown by the carbons in the aromatic rings with delocalized π bonding is beneficial to capture photogenerated electrons.[52] Therefore, the use of HSPHS as a TiO$_2$ catalyst scaffold exhibited a very high photocatalytic activity. On the other hand, the anatase TiO$_2$ supported on the polymer microspheres was not easily detached due to the coupled action of the sulfonic acid groups, which resulted in the excellent recyclability of the HSPHS@TiO$_2$-An because of the good adhesion between the titania and HSPHS scaffold.[43]

928 | *Mater. Chem. Front.*, 2019, **3**, 922–930

This journal is © The Royal Society of Chemistry and the Chinese Chemical Society 2019

Conclusions

Janus hollow polymeric hairy microspheres (HSPHS) were fabricated *via* cationic polymerization of DVB on the surface of SiO_2 cores, and then sulfonic acid groups ($-SO_3H$) were introduced onto the surface of the microspheres by sulfonation, followed by the removal of the SiO_2 cores *via* HF etching. The HSPHS can serve as efficient adsorbents for dye removal from wastewater. The isotherm and kinetics of dye adsorption using the HSPHS as adsorbents were investigated. Hydrophilic dye rhodamine B (RB) and hydrophobic dye dimethyl yellow (DMY) were used as model compounds. The results showed that >98% of RB or/and DMY could be removed from the surrounding solution within several minutes. The sulfonic acid groups on the HSPHS surface facilitated the further loading of titania, and thus the HSPHS can also serve as catalyst scaffolds for the photocatalytic degradation of RB. Anatase titania loaded HSPHS (HSPHS@TiO_2-An) demonstrated a remarkable photocatalytic efficiency and recyclability. High photocatalytic activity was observed for HSPHS@TiO_2-An under light irradiation of 30 W even when the initial concentration of RB was up to 300 mg L^{-1}. After five catalytic cycles, the catalytic efficiency remained similar to that of the first cycle with no loss of the photocatalytic activity. Thus, the HSPHS have promising potential in water treatment as efficient adsorbents and catalyst scaffolds.

Conflicts of interest

There are no conflicts to declare.

Acknowledgements

Notes and references

1 X. Wang, R. Ma, D. Cui, Q. Cao, Z. Shan and Z. Jiao, *Sci. Rep.*, 2017, **7**, 14233.

2 G. Bayramoğlu and M. Y. Arica, *J. Hazard. Mater.*, 2007, **144**, 449.

3 H. Sadegh, G. A. M. Ali, V. K. Gupta, A. S. H. Makhlouf, R. Shahryari-ghoshekandi, M. N. Nadagouda, M. Sillanpää and E. Megiel, *J. Nanostruct. Chem.*, 2017, **7**, 1.

4 M. A. Shannon, P. W. Bohn, M. Elimelech, J. G. Georgiadis, B. J. Marinas and A. M. Mayes, *Nature*, 2008, **452**, 301.

5 B. E. Barragan, C. Costa and M. C. Marquez, *Dyes Pigm.*, 2007, **75**, 73.

6 A. B. dos Santos, F. J. Cervantes and J. B. van Lier, *Bioresour. Technol.*, 2007, **98**, 2369.

7 C. T. M. J. Frijters, R. H. Vos, G. Scheffer and R. Mulder, *Water Res.*, 2006, **40**, 1249.

8 J. Zhang, Q. Shi, C. Zhang, J. Xu, B. Zhai and B. Zhang, *Bioresour. Technol.*, 2008, **99**, 8974.

9 V. K. Gupta, R. Jain and S. Varshney, *J. Colloid Interface Sci.*, 2007, **312**, 292.

10 F. Liu, Z. Guo, H. Ling, Z. Huang and D. Tang, *Microporous Mesoporous Mater.*, 2016, **227**, 104.

11 X. Peng, D. Huang, T. Odoom-Wubah, D. Fu, J. Huang and Q. Qin, *J. Colloid Interface Sci.*, 2014, **430**, 272.

12 Y. Ning, Y. Yang, C. Wang, T. Ngai and Z. Tong, *Chem. Commun.*, 2013, **49**, 8761.

13 I. Ali, *Chem. Rev.*, 2012, **112**, 5073.

14 M. Rafatullah, O. Sulaiman, R. Hashim and A. Ahmad, *J. Hazard. Mater.*, 2009, **170**, 969.

15 V. K. Gupta and Suhas, *J. Environ. Manage.*, 2009, **90**, 2313.

16 A. Ahmad, M. Rafatullah and M. Danish, *Holz Roh – Werkst.*, 2007, **65**, 429.

17 A. Ahmad, M. Rafatullah, O. Sulaiman, M. H. Ibrahim, Y. Y. Chii and B. M. Siddique, *Desalination*, 2009, **247**, 636.

18 B. Pan, B. Pan, W. Zhang, L. Lv, Q. Zhang and S. Zheng, *Chem. Eng. J.*, 2009, **151**, 19.

19 E. N. El Qada, S. J. Allen and G. M. Walker, *Chem. Eng. J.*, 2008, **135**, 174.

20 E. GilPavas, I. Dobrosz-Gomez and M. A. Gomez-Garcia, *Sci. Total Environ*, 2019, **651**, 551.

21 T. S. Kazeem, S. A. Lateef, S. A. Ganiyu, M. Qamaruddin, A. Tanimu, K. O. Sulaiman, S. M. S. Jillani and K. Alhooshani, *J. Cleaner Prod.*, 2018, **205**, 303.

22 S. Sivalingam, T. Kella, M. Maharana and S. Sen, *J. Cleaner Prod.*, 2019, **208**, 1241.

23 T. T. N. Phan, A. N. Nikoloski, P. A. Bahri and D. Li, *J. Environ. Manage.*, 2018, **233**, 471.

24 S. M. S. Arabi, R. S. Lalehloo, M. R. T. B. Olyai, G. A. M. Ali and H. Sadegh, *Phys. E*, 2019, **106**, 150.

25 L. Wang, W. Liu, T. Wang and J. Ni, *Chem. Eng. J.*, 2013, **225**, 153.

26 X. Yang and H. Liu, *Chem. – Eur. J.*, 2018, **24**, 13504.

27 K. Zheng, B. Pan, Q. Zhang, W. Zhang, B. Pan, Y. Han, Q. Zhang, D. Wei, Z. Cu and Q. Zhang, *Sep. Purif. Technol.*, 2007, **57**, 250.

28 H. P. C. van Kuringen, G. M. Eikelboom, I. K. Shishmanova, D. J. Broer and A. P. H. J. Schenning, *Adv. Funct. Mater.*, 2014, **24**, 5045.

29 Y. Xie, T. Wang, X. Liu, K. Zou and W. Deng, *Nat. Commun.*, 2013, **4**, 1960.

30 S. Ding and W. Wang, *Chem. Soc. Rev.*, 2013, **42**, 548.

31 L. Tan and B. Tan, *Chem. Soc. Rev.*, 2017, **46**, 3322.

32 J. Germain, J. Hradil, J. M. J. Frechet and F. Svec, *Chem. Mater.*, 2006, **18**, 4430.

33 N. M. Mahmoodi, F. Najafi and A. Neshat, *Ind. Crops Prod.*, 2013, **42**, 119.

34 D. D. Maksin, A. B. Nastasovic, A. D. Milutinovic-Nikolic, L. T. Surucic, Z. P. Sandic, R. V. Hercigonja and A. E. Onjia, *J. Hazard. Mater.*, 2012, **209**, 99.

35 T. Yao, S. Guo, C. Zeng, C. Wang and L. Zhang, *J. Hazard. Mater.*, 2015, **292**, 90.

This journal is © The Royal Society of Chemistry and the Chinese Chemical Society 2019

Mater. Chem. Front., 2019, **3**, 922–930 | **929**

36 D. Chen, Y. Liu, Y. Qin, L. Wang, Y. Ma and W. Yang, *Chin. J. Chem.*, 2017, **35**, 596.

37 Y. Ning, C. Wang, T. Ngai and Z. Tong, *Langmuir*, 2013, **29**, 5138.

38 Y. Wang, Y. Li, S. Liu and B. Li, *Carbohydr. Polym.*, 2015, **120**, 53.

39 Y. Yang, H. Liao, Z. Tong and C. Wang, *Compos. Sci. Technol.*, 2015, **107**, 137.

40 M. He, Q. Zhang, X. Zeng, D. Cui, J. Chen, H. Li, J. Wang and Y. Song, *Adv. Mater.*, 2013, **25**, 2291.

41 T. Hasell, H. Zhang and A. I. Cooper, *Adv. Mater.*, 2012, **24**, 5732.

42 M. Rafatullah, O. Sulaiman, R. Hashim and A. Ahmad, *J. Hazard. Mater.*, 2010, **177**, 70.

43 L. Zhang, P. Liu and Z. Su, *J. Mater. Sci.*, 2006, **41**, 7218.

44 J. Yu, G. Dai and B. Cheng, *J. Phys. Chem. C*, 2010, **114**, 19378.

45 Y. Chen, Z. Liu, X. Qu, F. Liang and Z. Yang, *Chem. – Asian J.*, 1785, **2016**, 11.

46 Y. Tang, L. Liu, X. Wang, D. Jia, W. Xia, Z. Zhao and J. Qiu, *J. Power Sources*, 2016, **319**, 227.

47 K. Lv and Y. Xu, *J. Phys. Chem. B*, 2006, **110**, 6204.

48 K. Lv, X. Guo, X. Wu, Q. Li, W. Ho, M. Li, H. Ye and D. Du, *Appl. Catal., B*, 2016, **199**, 405.

49 K. Lv, J. Yu, K. Deng, J. Sun, Y. Zhao, D. Du and M. Li, *J. Hazard. Mater.*, 2010, **173**, 539.

50 B. Pan, Q. Zhang, F. Meng, X. Li, X. Zhang, J. Zheng, W. Zhang, B. Pan and J. Chen, *Environ. Sci. Technol.*, 2005, **39**, 3308.

51 J. Yu and B. Wang, *Appl. Catal., B*, 2010, **94**, 295.

52 L. Zhang, H. Gao and Y. Liao, *J. Mater. Sci.*, 2016, **51**, 10585.